https://doi.org/10.1016/j.matlet.2022.133339

A novel $L1_2$-strengthened AlCoCuFeNi high-entropy alloy with both high strength and good corrosion resistance

Yaojia Ren [a], Hong Wu [a], Bin Liu [a], Quan Shan [b], Sheng Guo [c], Zengbao Jiao [d], Ian Baker [e]

a. State Key Laboratory of Powder Metallurgy, Central South University, Changsha 410083, China
b. Academy of Materials Science and Engineering, Kunming University of Science and Technology, Kunming, China
c. Department of Industrial and Materials Science, Chalmers University of Technology, Gothenburg SE-41296, Sweden
d. Department of Mechanical Engineering, The Hong Kong Polytechnic University, Hong Kong 999077, China
e. Thayer School of Engineering, Dartmouth College, Hanover, NH 03755-8000, USA

Abstract

In this work, crack-free AlCoCuFeNi high-entropy alloys with high strength and good corrosion corrosion resistance were successfully fabricated using spark plasma sintering (SPS) and hot rolling. The microstructure of the specimen is composed of a fine equiaxed grains of Al-enriched BCC, Cu-enriched FCC, Fe-enriched $L1_2$, and Al_2O_3 phases. The maximum texture index is only 1.53, indicating the low anisotropy of the material. The specimens possessed the high hardness (~599 HV) combined with excellent comprehensive corrosion resistance, which is comparable to the specimen prepared by laser metal deposition. In addition, the creep mechanism for the specimen is governed by grain boundary sliding.

Keywords: High entropy alloy, microstructure, nanomechanics, corrosion resistance.

1. Introduction

Copper-containing high entropy alloys (HEAs) have attracted great interest due to their high antimicrobial efficiency, good wear resistance and good corrosion resistance [1, 2]. However, Cu has a strong tendency to segregate in AlCoCuFeNi HEAs due to the positive mixing enthalpy of Cu with other alloying elements [3]. Further, diffusion anneals do not eliminate the Cu segregation. Laser metal deposition (LMD) technology has the advantages of short process times, high efficiency and low cost, and has been widely used in the rapid preparation of alloys [4]. This technology exhibits excellent macrosegregation suppression due to its high cooling rate. Unfortunately, LMD-processed AlCoCuFeNi HEAs inevitably suffer from the presence of cracks formed due to the solidification shrinkage of Cu-rich thin films [5]. This means that the preparation of AlCoCuFeNi HEAs using LMD, in which a liquid to solid state transformation occurs, is less than ideal. Spark plasma sintering (SPS), a preparation method that does not involve the liquid state, also shows the potential to avoid segregation. Due to the fast heating rates (~50℃/min), short sintering times (~5 mins), and concurrent application of uniaxial pressure, this technology can be used to control the microstructure by inhibiting grain growth, and can be used to form high-density, crack-free samples [6]. However, the properties of SPS-processed samples are normally not comparable to LMD-processed samples. This is due to the superior work hardening ability of the latter. To obtain a high strength, corrosion resistant and crack-free AlCoCuFeNi HEA, SPS with rapid prototyping ability was employed in this work followed by hot rolling. The phases present, the microstructure,

the element segregation, the nanomechanical properties, and the corrosion behavior of the AlCoCuFeNi were investigated in detail. This work provided a basis for the preparation of high performance of Cu-containing HEAs.

2. Experimental

The prealloyed powders were consolidated by SPS furnace (FCT D25/3, Germany) in graphite die at a sintering temperature of 1000°C. Other detailed conditions were described elsewhere. The specimen was held at 600°C for 30 min and then hot rolled with a reduction of 10%. Phase identification was performed using a Bruker D8 Advance X-ray diffractometer with Cu-Kα radiation. The microstructure was examined using a scanning electron microscope (SEM, Nova NanoSEM 230) equipped with an electron backscatter diffraction (EBSD), and a transmission electron microscope (TEM, FEI Talos F200x) equipped with an energy dispersive spectrometer (EDS). An electron probe micro-analyzer (EPMA) was used to determine the elemental segregation. Nanoindentation measurements were conducted at room temperature with a peak load of 30 mN and a dwell time of 15s. Creep test were also performed with a dwell time of 600s. Nano scratch tests were performed using a peak load and scratch distance of 500 mN and 200 μm, respectively. Corrosion tests were performed in a 3.5wt.% NaCl solution using a standard three-electrode system (Gamry reference 600+, America) with a specimen exposure area of 1 cm^{-2}.

3. Results and discussion

An XRD pattern from the rolled AlCoCuFeNi HEAs is shown in Fig. 1a. This indicates that the specimen consists of BCC and FCC phases. A phase distribution map is shown in Fig. 1b, in which the BCC phase is colored red, and the FCC phase is colored blue. It can be seen that the FCC phase is randomly distributed. Fig. 1c is an inverse pole figure (IPF) of the specimen showing that the grain size is ~1 μm. Since there is no heat source in the sintering process to induce directional grain growth, equiaxed grains with low anisotropy are obtained, and the maximum texture index is only 1.53, see Fig. S1. The corresponding kernel average misorientation (KAM) map in Fig. 1d shows that the internal stress of the HEAs is not high even after 10% hot rolling. The sintering process does not involve liquid phase, which prevents the formation of hot cracking. The low cooling rates and limited deformation make the specimen also free from cold cracking, see Fig. S2. The fraction of low-angle grain boundaries (LAGBs) in the specimen prepared by SPS and hot rolling is 35% in the BCC phase and 61 % in the FCC phase, as shown in Fig. S3.

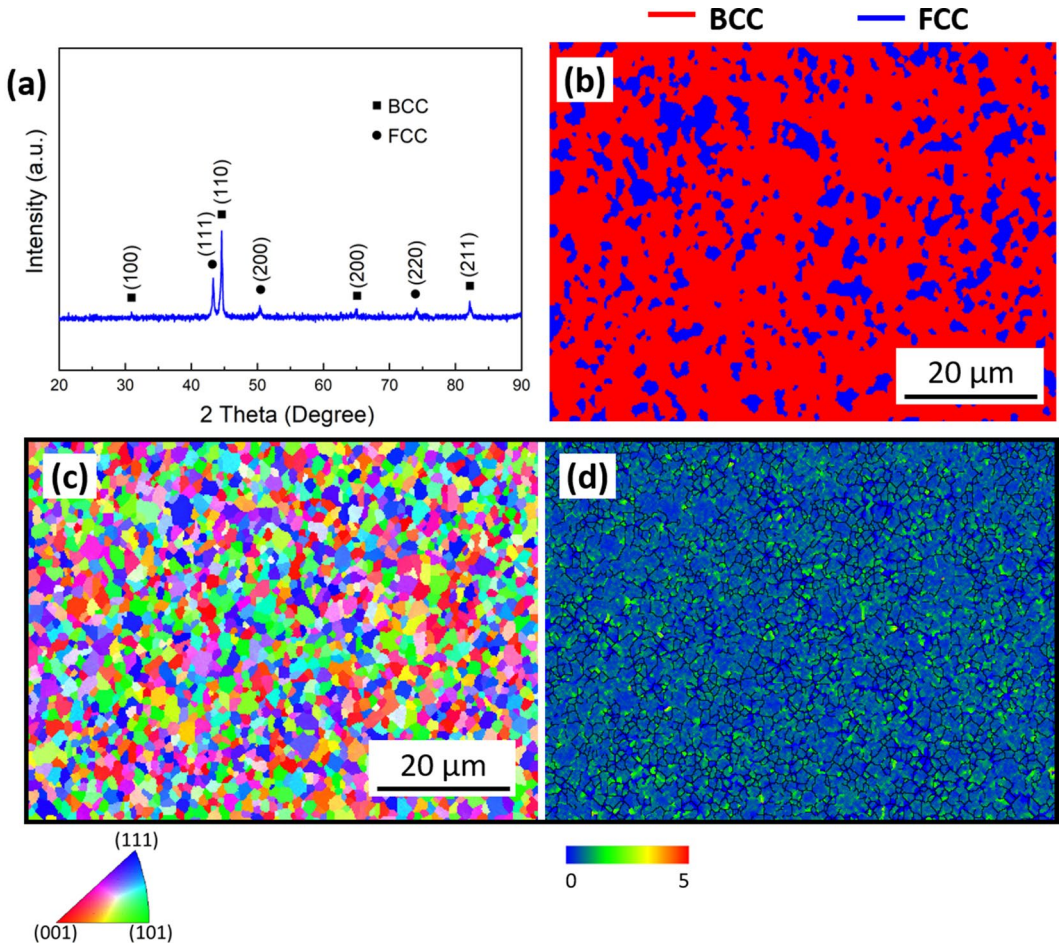

Fig. 1 (a) XRD pattern, (b) phase distribution map, (c) IPF map, and (d) KAM map of AlCoCuFeNi HEA.

A back-scattered electron (BSE) image and corresponding Fe, Co, Ni, Cu, and Al elemental distributions from the rolled specimen are shown in Fig. 2. Well-bonded ultrafine grains can be clearly seen. Because the sintering temperature is close to the melt point of the Cu and Al, the segregation of Cu and Al elements is considerable. The enrichment of Cu in the fine-grained zone is particularly evident. Note the segregation of Cu is on a small scale, which which means that the composition is homogeneous on a macroscale. Combined with Fig. 1b, it can be inferred that the Cu-rich fine-grained zone is mainly the FCC phase. The transformation from the BCC

phase to the FCC phase dissipates energy and, thus, inhibits the grain growth.

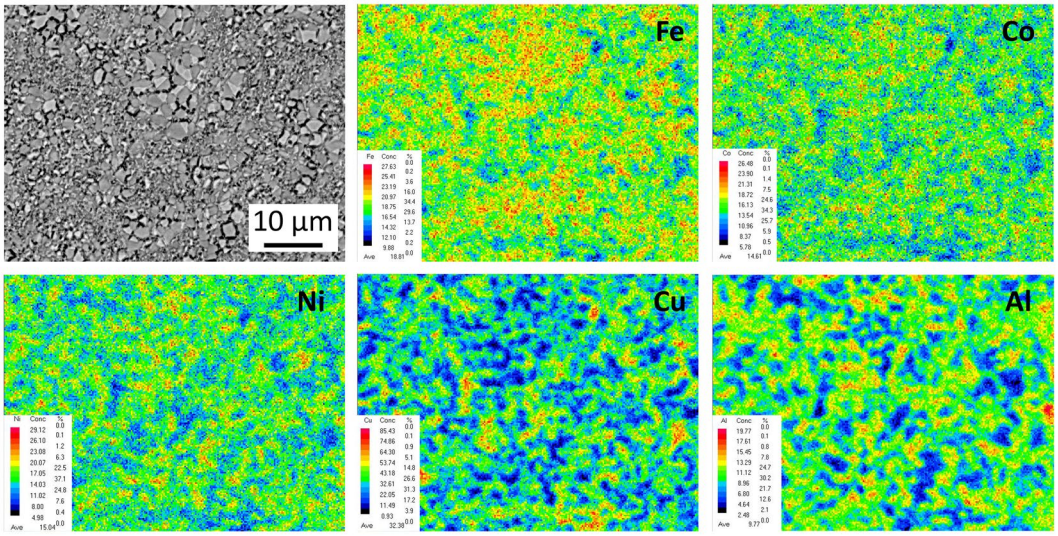

Fig. 2 BSE image and corresponding EPMA micrographs of AlCoCuFeNi HEA.

Fig. 3a is a bright field (BF) image showing fine-grain equiaxed grains in the rolled specimen. A high-angle annular dark-field (HAADF) image and corresponding elemental X-ray maps of Fe, Co, Ni, Cu, Al, and O are shown in Fig. 3b and 3d, respectively. It is clear that a Cu-enriched FCC phase and an Al-enriched BCC phase are formed. In addition, nano-scale chemical inhomogeneity of Cu, Fe, Ni and Co can be observed in the Cu-rich region. To further indicate the nano-scale chemical segregation, an EDS line scan was taken from the red line in Fig. 3b. This shows that the Al is nearly homogeneously distributed in the Cu-rich FCC phase. Compared with the Fe and Co, the partitioning of Ni is relatively weak. The Fe-, Co-, and Cu-rich regions can be clearly distinguished. A high-resolution TEM (HRTEM) image of the precipitates is shown in Fig.3c. The inset SAED pattern shows a $L1_2$ phase viewed along [0-11] - the arrowed (100) diffraction spot indicates the ordering. Generally, in terms of kinetics, it is easier to form a FCC phase through Cu uphill diffusion than the

$L1_2$ phase, because the latter requires the rearrangement of multiple elements (Fe, Co and Ni). The SPS-processed AlCoCuFeNi HEA is composed of BCC and FCC dual phases [7]. While the hot rolling promotes the spinodal decomposition and leads to the $L1_2$ ordering. Al-rich oxides can be clearly observed along the grain boundary in Fig. 3d. Combined with the corresponding EDS line scan in Fig. S4, this precipitate is probably Al_2O_3. It is formed when exposed to the atmosphere during hot rolling.

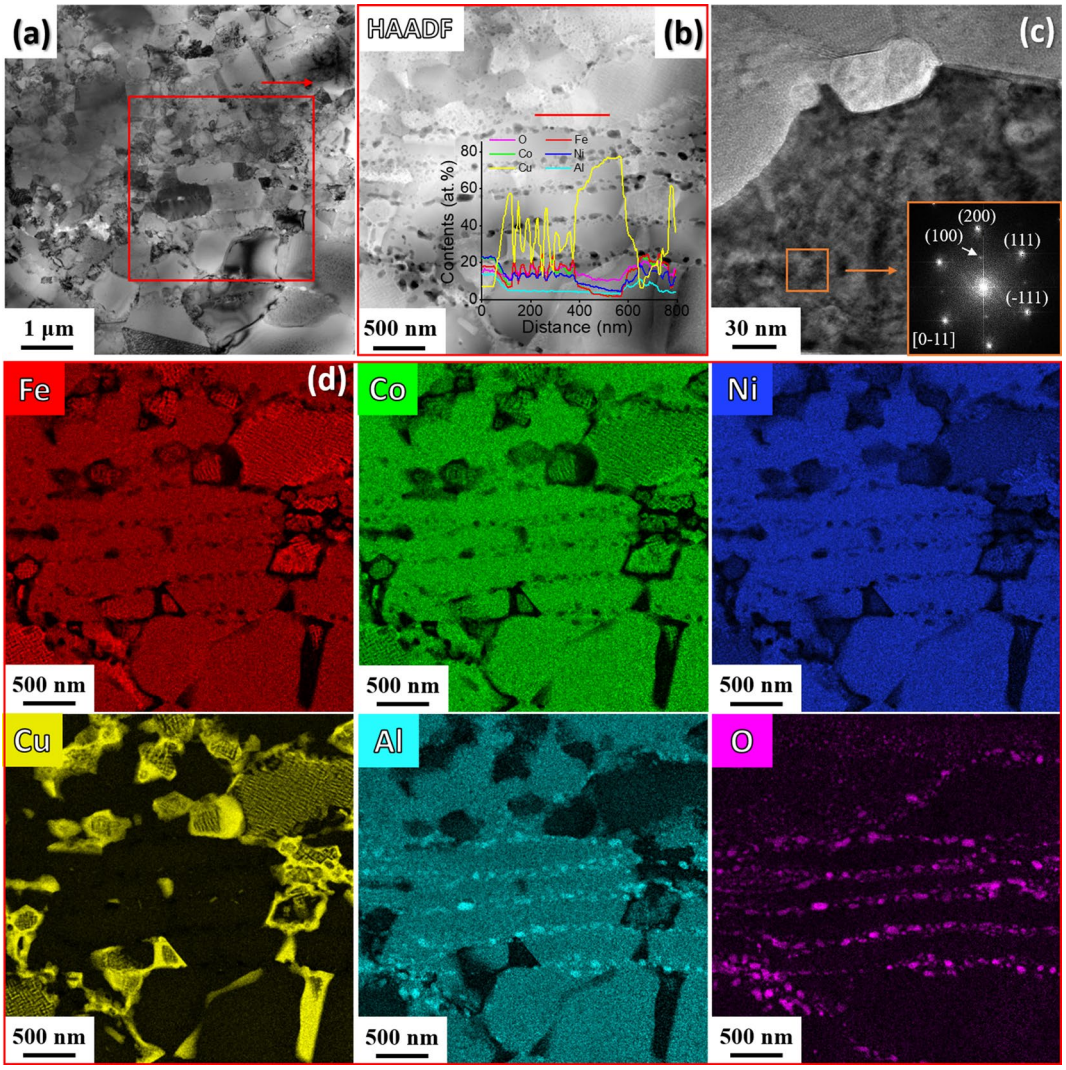

Fig. 3 TEM analysis of the rolled AlCoCuFeNi HEA: (a) BF image; (b) HAADF image taken from (a), and corresponding EDS line scan obtained from the red line; (c) HRTEM image of the precipitates, and the inset [0-11] SAED pattern; (d) X-ray maps

of Fe, Co, Ni, Cu, Al, and O corresponding to HAADF image in (b).

The hardness and of the rolled AlCoCuFeNi specimen was 599 ± 30 HV, which is slightly higher than that of LMD-processed specimens [5]. This hardness increase is mainly attributed to the $L1_2$ phase and refined grains, supplemented by Al_2O_3 oxides. The scratch test enters the steady-state wear stage as soon as the Rockwell diamond indenter contacts with the alloy surface, as shown in Fig. 4a. The average friction coefficient was approximately 0.1, which is lower than that of LMD-processed specimens. Fig. 4b is the typical scratched surface of the AlCoCuFeNi specimen. The scratch width is about 14 μm, which is similiar to that of an LMD-processed specimen [5]. This means that the wear resistance of the AlCoCuFeNi specimen prepared by SPS and hot rolling is comparable to that of the LMD-processed specimen.

The creep displacement of the specimen as a function of time is shown in Fig. 4c. The blue region reflects the creep stage. Details of the calculation method for the creep stress exponent (n) are described elsewhere [8]. The fitted logarithmic plot present in Fig. 4d shows that the n value of the AlCoCuFeNi specimen is about 2. This indicates that the creep mechanism is dominated by the grain boundary sliding, and its creep resistance would be expected to be lower than that of a LMD-processed specimen [5].

The corrosion potential (E_{corr}) of the specimen is about -0.27 V, as shown in Fig. 4e. The corrosion current density (i_{corr}) is calculated to be 1.13 μA cm^{-2} using an extrapolation method. The corrosion preferentially occurs in Cu-rich region, as shown

in Fig. 4f. The fine grain size could enhance the surface energy, thereby promoting the formation of passivation films. The formation of $L1_2$ phase can inhibit the migration of LAGBs and improve the corrosion resistance [9].

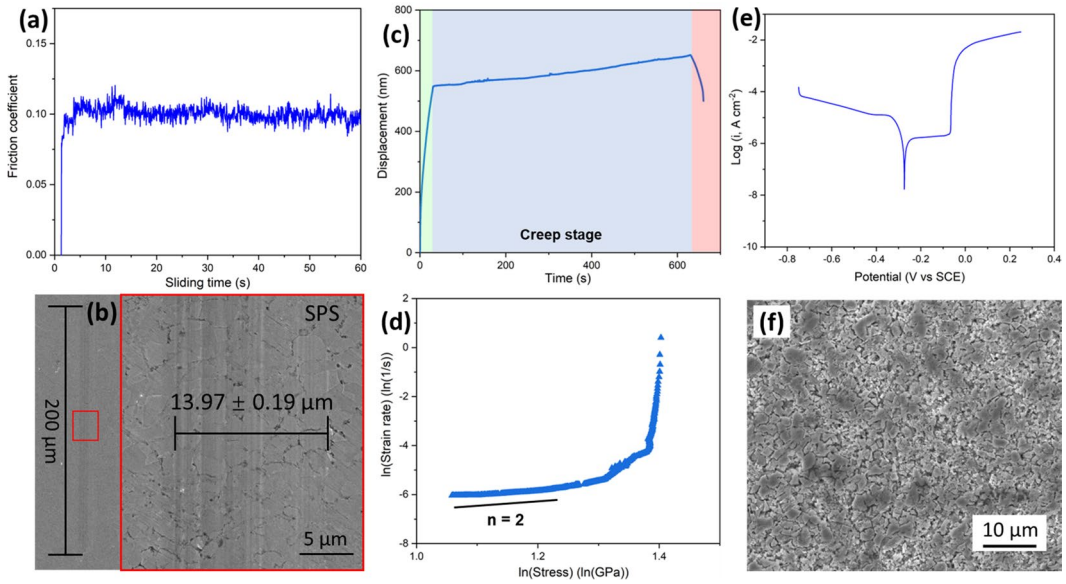

Fig. 4 (a) Friction coefficient, (b) secondary electron (SE) image of the scratched surface, (c) displacement versus time plot, (d) fitted logarithmic plot, (e) tafel curve, (f) SE image of the corrode surface.

4. Summary

AlCoCuFeNi HEA prepared by consolidation of pre-alloyed powder using SPS followed hot rolling consisted of fine (~1 µm), randomly-oriented, equiaxed grains of Al-enriched BCC, Cu-enriched FCC, $L1_2$, and Al_2O_3 phases. The hardness of the specimen is 599 ± 30 HV, and the material possesses a good wear resistance. The creep mechanism of the specimen is mainly controlled by grain boundary sliding. The rolled HEA exihibits good corrosion resistance in 3.5 wt.% NaCl solution with a E_{corr} of -0.27 V and an i_{corr} of 1.13 µA cm^{-2}.

Acknowledgements

This work was supported by the National Natural Science Foundation of China (No. 52111530193) and the Key Research and Development Program of Hunan Province (No. 2022SK2006). The authors would also thank Sinoma Institute of Materials Research (Guang Zhou) Co., Ltd. for the assistance with the TEM characterization.

Reference

[1] W. Fu, Y. Huang, J. Sun, A.H. Ngan, International Journal of Plasticity, 154 (2022) 103296.
[2] M. Zhang, X. Zhou, D. Wang, L. He, X. Ye, W. Zhang, Journal of Alloys and Compounds, 893 (2022) 162259.
[3] Y. Ren, L. Liang, Q. Shan, A. Cai, J. Du, Q. Huang, S. Liu, X. Yang, Y. Tian, H. Wu, Virtual and Physical Prototyping, 15 (2020) 543-554.
[4] Y. Ren, J. Du, B. Liu, Z. Jiao, Y. Tian, I. Baker, H. Wu, Materials Science and Engineering: A, (2022) 143402.
[5] Y. Ren, H. Wu, B. Liu, Y. Liu, S. Guo, Z. Jiao, I. Baker, Journal of Materials Science & Technology, (2022).
[6] Y. Yang, Y. Ren, Y. Tian, K. Li, W. Zhang, Q. Shan, Y. Tian, Q. Huang, H. Wu, Journal of Alloys and Compounds, 884 (2021) 161070.
[7] Y. Long, G. Li, X. Liang, H. Peng, Frontiers in Materials, 7 (2020) 537812.
[8] W. He, Q. Zeng, C. Yan, J. Zhu, D. Zhang, J. Cao, Journal of Materials Science & Technology, 101 (2022) 173-186.
[9] H. Zhong, S. Li, Z. Zhang, D. Li, H. Deng, J. Chen, L. Qi, O.A. Ojo, Materials Today Communications, (2022) 103732.